Time-energy analysis of above-threshold ionization in few-cycle laser pulses

L. Guo and S. S. Han

Key Laboratory for Quantum Optics, Center for Cold Atom Physics, Shanghai Institute of Optics and Fine Mechanics, Chinese Academy of Sciences, Shanghai 201800, China

J. Chen*

HEDPS, Center for Applied Physics and Technology, Peking University, Beijing 100084, China

Institute of Applied Physics and Computational Mathematics, P.O. Box 8009, Beijing 100088, China

(Received 21 August 2012; published 13 November 2012)

A Wigner-distribution-like (WDL) function is used to study the time-energy distribution of a photoelectron emitted from an atom in few-cycle laser fields with different frequencies. The WDL function shows the dependence of ionization probability on time and explicitly demonstrates the transition of the ionization process from the multiphoton regime to the tunneling regime with decreasing laser frequency. Accompanying this transition, the semiclassical relationship between the final drift energy and the ionization moment becomes more and more valid and is in good agreement with the time-energy distribution in the tunneling regime. Meanwhile, the photoelectron energy spectrum shows a fine structure, which is more and more dependent on the direction of the ejection of the photoelectron and the carrier-envelope phase of the laser field. Moreover, the WDL function enables us to explicitly attribute the fine structure in the tunneling regime to interference between electrons with the same kinetic energy ejected at different times.

DOI: 10.1103/PhysRevA.86.053409 PACS number(s): 32.80.Rm, 32.80.Fb

I. INTRODUCTION

Above-threshold ionization (ATI) is a fundamental process in strong-field atomic physics. The corresponding physical process is known to be usually categorized into two distinct regimes: multiphoton ionization and tunneling ionization. These two regimes are distinguished by the Keldysh parameter $\gamma = \sqrt{I_p/2U_p}$ (I_p is the ionization potential, and $U_p = I/4\omega^2$ denotes the ponderomotive energy, where I is the laser intensity and ω is the frequency) [1]. When γ is well above 1, the ionization process is in the multiphoton regime, and the ATI energy spectrum consists of a series of regularly spaced narrow peaks, each separated by one-photon energy [2]. When γ decreases to be less than 1, the ionization process enters the tunneling regime in which the ionization can be understood in a quasistatic picture: The electron tunnels through a barrier formed by the ionic Coulomb potential and the external electric field, which is commonly known as the simple man's picture of the ATI process [3]. In the tunneling regime, the photoelectron energy spectrum shows a rather smooth distribution in which the ATI peaks are mostly smeared out by the focal average effect of the laser pulse. The overall spectrum consists of a fast drop in the low-energy regime followed by a plateau structure and a cutoff at about $10U_p$ in the high-energy regime [4,5]. This overall structure can be well interpreted by a rescattering mechanism based on the simple man's picture: Once the electron tunnels out of the barrier, it oscillates in the external laser field and may return back to collide with the core, which gives rise to the plateau and cutoff structures in the observed energy spectrum [4,6]. It is noteworthy that this semiclassical picture of the ATI process has also achieved great success in the description of other abnormal phenomena in an intense laser-atom interaction, e.g., plateau and cutoff in the high harmonic generation spectrum and nonsequential double ionization process. In addition, with the inclusion of the long-range ionic Coulomb potential, this semiclassical picture also well explains the recently observed low-energy structure in the ATI spectrum, which becomes pronounced in the midinfrared intense laser field [7,8].

On the other hand, the physical picture in quantum theory, corresponding to the above semiclassical perspective, is the so-called "quantum trajectory theory" [9]. In this approach, the transition amplitude is obtained by the coherent sum of various trajectories similar to those in the semiclassical picture discussed above. In the spirit of the path-integral picture of the quantum mechanics, this model successfully explains interference effects in the ATI process, e.g., resonancelike enhancement in the ATI plateau [10] and carrier-envelope phase (CEP) dependence of a high-energy photoelectron spectrum in few-cycle laser pulses [11,12].

Clearly, the above-mentioned semiclassical picture (or extended simple man's picture) of the ATI process is based on the availability of the following understanding: The electron is ionized by the laser field via tunneling for which the ionization probability is exponentially dependent on the amplitude of the electric field, and then the motion of the electron in the external field and the ionic potential can be treated classically, or in other words, there is a specific relationship between the electron's drift momentum and the corresponding ionization moment. However, this picture, which is under the quasistatic approximation of the ionization process, has never been explicitly depicted in any investigation despite the fact that it has been proved that, in the limit of $\gamma \ll 1$, the Keldysh-Faisal-Reiss formula of the ATI process [1,13,14] indeed agrees with the time-averaged tunneling ionization formula [14,15].

In this paper, we use a Wigner-distribution-like (WDL) function [16] to study the time-energy distribution of a photoelectron emitted from an atom in few-cycle laser fields

*chen_jing@iapcm.ac.cn

with different frequencies. The WDL function enables us to show the dependence of ionization probability on time and explicitly demonstrates the transition of the ionization process from the multiphoton regime to the tunneling regime with decreasing laser frequency, i.e., decreasing Keldysh parameter γ. Accompanying this transition, we explicitly show that the time-energy distribution evolves and is consistent with the semiclassical picture in the tunneling regime. Meanwhile, the photoelectron energy spectrum depicts a fine structure, which is more and more dependent on the direction of the ejection of the photoelectron and CEP of the laser field, which can be attributed to interference between electrons with the same kinetic energy ejected at different times in the tunneling regime.

II. THEORY

The Wigner-distribution-like function is defined as [16]

$$f\left(t,\frac{p^2}{2}\right)=\frac{1}{\pi}\int_{-\infty}^{\infty}S'^{*}(t+t')S'(t-t')e^{-2i(p^2/2)t'}dt', \quad (1)$$

where S' is given by

$$S'=\frac{-i\sqrt{2\pi}}{\sqrt{v}}\phi_i(\mathbf{p})V_A(\mathbf{p},t)\exp\left[i\int_{-\infty}^{t}V_A(\mathbf{p},\tau)d\tau+iI_pt\right]. \quad (2)$$

Here, v is the normalization volume, $V_A(\mathbf{p},t)$ is the interaction potential between the applied laser field and the photoelectron, $\phi_i(\mathbf{p})$ is the Fourier transform of $\varphi_i(t)$, which is the atomic ground state $|\varphi_0\rangle e^{iI_pt}$, and I_p is the ionization potential.

In this paper, we use a linearly polarized laser pulse with a $\sin^2$-type temporal envelope. The vector potential is given by

$$\mathbf{A}(\mathbf{t})=-\frac{E_0}{\omega}\sin^2\left[\frac{\omega t}{n}\right]\cos(\omega t+\varphi)\mathbf{e}_z, \quad (3)$$

where E_0 is the field peak strength, ω is the laser frequency, and $n/2$ is the number of optical cycles (o.c.) contained in the laser pulse. φ is the initial phase. $\mathbf{e}_z$ is the unit vector.

Under these conditions, we have

$$f\left(t,\frac{p^2}{2}\right)=\frac{1}{\pi}\int_{0}^{T_c}S'^{*}(t+t')S'(t-t')e^{-2i(p^2/2)t'}dt', \quad (4)$$

here, $T_c=\frac{\pi n}{\omega}$ is the duration of the pulse and velocity gauge used in this paper.

The WDL function $f(t,\frac{p^2}{2})$ satisfies the marginal relationship,

$$|S_{fi}|^2=\int f\left(t,\frac{p^2}{2}\right)dt, \quad (5)$$

where S_{fi} is given by $S_{fi}=\frac{1}{\sqrt{2\pi}}\int_{-\infty}^{\infty}S'e^{i(p^2/2)t}dt$.

Furthermore, one can find that the ionization probability as a function of time can be given by

$$P(t)=\int f\left(t,\frac{p^2}{2}\right)d\left(\frac{p^2}{2}\right). \quad (6)$$

III. RESULT AND DISCUSSION

At first, we calculate $P(t)$ for a one-dimensional H atom ($I_p=13.6$ eV) in a few-cycle laser pulse [with $n=8$ in Eq. (3)] at different wavelengths. As shown in Fig. 1, when the laser frequency is high ($\omega=0.5$ a.u.), the time distribution of the ionization probability shows a rather smooth envelope, which roughly resembles the shape of the laser pulse. When the laser frequency decreases to $\omega=0.182$ a.u., the ionization probability tends to peak at moments when the electric field reaches maxima [see Figs. 1(c) and 1(d)]. When ω decreases further to 0.056 91 a.u., the distribution already shows a typical tunneling pattern: The ionization probability is strongly dependent on the electric-field amplitude, leading only to very sharp peaks at the crests of the electric field, and the heights of the peaks are strongly dependent on the amplitude of the field maximum [see Figs. 1(e) and 1(f)]. If the laser frequency decreases further, the ionization probability becomes more sensitive to the field amplitude as shown in Figs. 1(g) and 1(h) with $\omega=0.030\,35$. It is noteworthy that the Keldysh parameters, corresponding to four different laser frequencies used in our calculation, are 9.35, 3.4, 1.06, and 0.56. So, our calculation explicitly shows that, accompanying the decrease in γ, the ionization probability becomes more

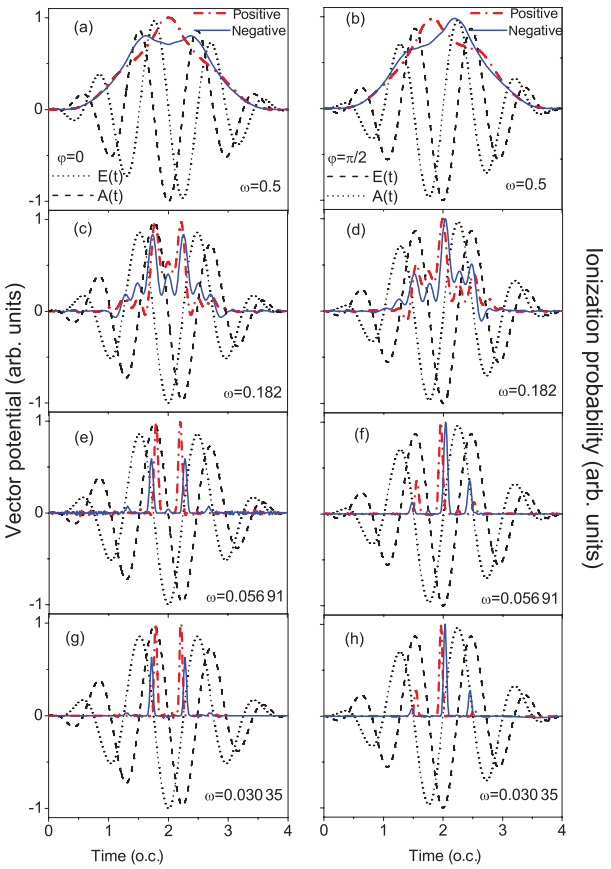

FIG. 1. (Color online) Calculated $P(t)$ of photoelectrons ejected in two oppositive directions in four-cycle laser pulses with different laser frequencies. Peak intensity $I=1\times10^{14}$ W/cm^2. The CEP $\varphi=0$ [(a), (c), (e), and (g)] and $\varphi=\pi/2$ [(b), (d), (f), and (h)]. Dashed-dotted red line: electron emitted in the positive direction; blue solid line: electron emitted in the negative direction.

and more strongly dependent on the field amplitude, which can be considered as a transition from the multiphoton regime to the tunneling regime. Moreover, it is worth noting that, strictly speaking, the tunneling picture of the ATI is only valid when $\gamma \ll 1$ [1,14,15]. However, the tunneling formula (or the semiclassical picture) is commonly used in an atom-intense laser interaction even when the Keldysh parameter is around 1 and the theoretical results are well consistent with the experimental observations [17]. According to our calculation, as explicitly shown in Figs. 1(e) and 1(f), the ionization process already shows a typical tunneling characteristic even when $\gamma \sim 1$, which is still far from the strict theoretical requirement that $\gamma \ll 1$. Therefore, the semiclassical model is already a valid approximation when γ is around 1.

It is obvious that the electric field of the few-cycle laser pulse is sensitive to the CEP and, more interestingly, shows either spatial asymmetry [e.g., see Fig. 1(a) for $\phi = 0$] or temporal asymmetry [e.g., see Fig. 1(b) for $\phi = \pi/2$], depending on the CEP. As a consequence, the ionization probability shows asymmetries in the positive and negative directions of electron emission and the temporal distribution with respect to the central moment of the pulse ($t = 2$ o.c. in Fig. 1). This asymmetry also shows an interesting transition when the ionization process transits from the multiphoton regime to the tunneling regime. In the typical multiphoton regime, e.g., $\omega = 0.5$ a.u. ($\gamma = 9.35$), the ionization probability shows slightly CEP-dependent spatial and temporal asymmetries [Figs. 1(a) and 1(b)]. With decreasing laser frequency and corresponding γ, the asymmetry becomes more and more distinct as shown in Figs. 1(c)–1(h).

Next, we investigate the energy spectrum and the two-dimensional time-energy distribution of the ATI process in a few-cycle laser pulse. The results are shown in Fig. 2, which also depicts an interesting transition when the ionization process transits from the multiphoton regime to the tunneling regime. In the multiphoton regime, the energy spectra show smooth ATI peaks and nearly no difference in the positive and negative directions [see Figs. 2(a)–2(d)]. Meanwhile, the time-energy distributions show a slight difference in two different directions corresponding to the ionization probability depicted in Fig. 1. When the laser frequency decreases to $\omega = 0.056\,91$ and $0.030\,35$ a.u., both the energy spectrum and the time-energy distribution become strongly dependent on the emission direction. More interestingly, the energy spectrum shows complicated interference patterns, which can be attributed to the interference between electrons with the same final drift kinetic energies but are ionized at different moments [10,11,18]. Clearly, this physical picture is only valid in the tunneling regime in which the electron with a specific final drift energy can be considered to be ionized at a specific moment. This point will be further illustrated in the following analysis.

First, we analyze the results of CEP $\varphi = 0$. In Figs. 2(e) and 2(g), two stripes appear next to the moments of $t = 2.25$ and $t = 1.75$ o.c. It is noteworthy that these two stripes are not perpendicular to the time axis. They gradually incline symmetrically to the center with increasing kinetic energy. Figures 2(f) and 2(h) show the time-energy distribution of the photoelectrons emitted in the negative direction. Two strips also appear next to $t = 2.25$ and $t = 1.75$ o.c., respectively, but they symmetrically incline off with increasing kinetic

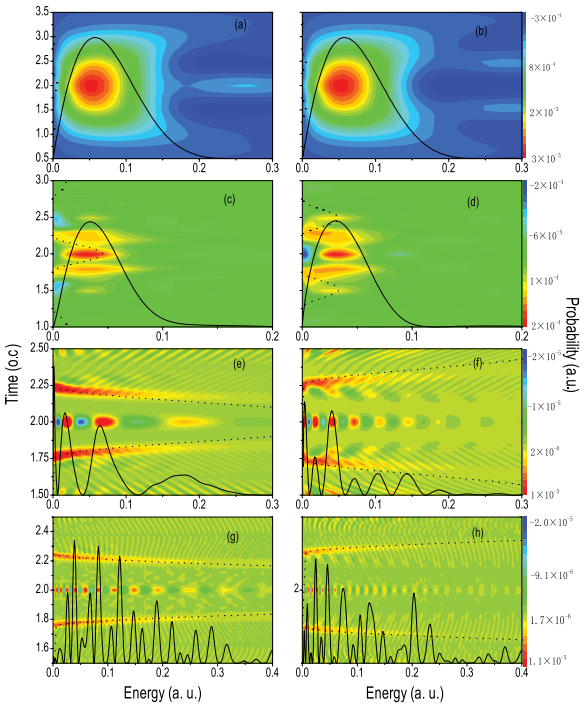

FIG. 2. (Color online) Time-energy distribution and energy spectrum (solid line) in few-cycle laser pulses with the CEP $\varphi = 0$. The laser parameters are the same as those used in Fig. 1. (a), (c), (e), and (g) An electron ejected in the positive direction; (b), (d), (f), and (h) an electron ejected in the negative direction. Dotted lines show the semiclassical relationship between the drift kinetic energy and the ionization moment [$p^2/2 = A^2(t)/2$].

energy, which is opposite to those shown in Figs. 2(e) and 2(g). Interestingly, it can be seen that there are some interference structures located in the center of the time-energy distribution (around $t = 2$ o.c.) in Figs. 2(e)–2(h). The negative maxima and positive maxima are in accordance with the minima and maxima in the energy spectra, respectively. Moreover, there are more interference structures in the low-frequency cases [Figs. 2(g) and 2(h)] than in the high-frequency cases [Figs. 2(e) and 2(f)]. In addition, the interference pattern becomes denser in the negative direction of electron emission [Figs. 2(f) and 2(h)] than in the positive direction [Figs. 2(e) and 2(g)] in accordance with the energy spectra.

The interference structures shown in Figs. 2(e)–2(h) can be attributed to the interference between the two strips started at $t = 2.25$ and $t = 1.75$ o.c. It is worth noting that the interference effect in the ATI spectrum in the few-cycle laser pulse has been discussed in Ref. [11], which attributes the fringes in the high-energy part of the ATI spectrum to the double-slit interference effect. A similar mechanism can be applied to explain the interference in Fig. 2. As shown in Figs. 2(e)–2(h) [see also Figs. 1(e)–1(h)], only electrons ionized around $t = 2.25$ and $t = 1.75$ o.c. contribute dominatingly to the energy spectrum, and the electrons ionized at other moments contribute negligibly since the ionization probability is strongly dependent on the electric amplitude in this regime. Similar to Ref. [11], Fig. 3 shows the electric field and vector potential of the laser pulse for $\phi = 0$. One can see that the interference comes from the electrons with the same

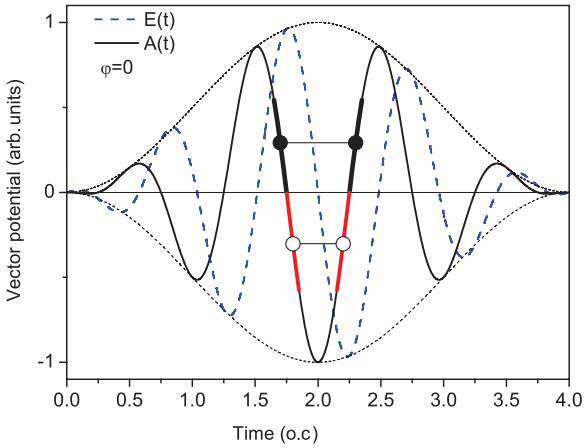

FIG. 3. (Color online) Vector potential and electric field of a four-cycle pulse with the initial phase $\varphi = 0$.

kinetic energy ejected at different times within the half-cycle from $t = 1.5$ to $t = 2.5$ o.c. (see Fig. 3). According to the semiclassical picture of the ATI process [6], the electron's drift momentum satisfies $\mathbf{P} = -\mathbf{A}$ in the tunneling regime, hence, the interference between the electrons emitted at the time shown by the red line in Fig. 3 results in the structures in Figs. 2(e) and 2(g) [see also the dotted lines in Figs. 2(e) and 2(g)]. The interference structures in Figs. 2(f) and 2(h) result from the interference between the electrons produced at the time shown by the bold black line in Fig. 3 [see also the dotted lines in Figs. 2(f) and 2(h)]. The difference between interference patterns in Figs. 2(e) and 2(f) [Figs. 2(g) and 2(h)] is due to the different energy dependence of the time interval in two directions: The time interval decreases with increasing energy in Fig. 2(e) [Fig. 2(g)] but increases with increasing energy in Fig. 2(f) [Fig. 2(h)].

Clearly, this mechanism is only applicable when the semiclassical picture of the ionization process is valid, or in other words, there is a correspondence between the kinetic energy and the ionization moment when the electron is ionized in the laser pulse, which is only available in the tunneling regime [or close to tunneling regime as shown in Figs. 1(e) and 1(f)]. In the multiphoton regime, as shown in Figs. 2(a)–2(d), the ionization probability of an electron with a specific energy distributes in a rather wide time regime, which means that the correspondence between the drift kinetic energy and the ionization moment does not exist, and hence, the interference pattern is smeared out by the large uncertainty in the time distribution of the ionization probability.

Last but not least, Fig. 2 also shows the evolution of the availability of the semiclassical picture of the ATI with the Keldysh parameter. In Figs. 2(a)–2(d), which are well in the multiphoton regime ($\gamma > 1$), the time-energy distributions show nearly no correspondence between the final drift momentum (or final drift energy) and the ionization moment and are hardly comparable to the semiclassical relationship [the curves of $p^2/2 = A^2(t)/2$]. It is noteworthy that, for $\omega = 0.5$ a.u., the drift energy ($2U_p = 0.0057$ a.u.), calculated by $p^2/2 = A^2(t)/2$, is too small to be distinguished in Figs. 2(a) and 2(b). In Figs. 2(e) and 2(f) for which $\gamma \sim 1$, although the time-dependent ionization probability already shows a typical tunneling ionization characteristic, the approximate correspondence between the final drift momentum and the ionization moment [represented by the strips in, i.e., Fig. 2(e)] still differs from the semiclassical relationship $\mathbf{P} = -\mathbf{A}$ noticeably, especially when the energy is high, which can be seen in Figs. 2(e) and 2(f) where the strips diverge from the dotted lines noticeably when $E_k > 0.1$ a.u. It is noteworthy that, only in Figs. 2(g) and 2(h) for which the Keldysh parameter well satisfies $\gamma < 1$, the energy-time dependence is in good agreement with the semiclassical relationship [the strips in Figs. 2(g) and 2(h) coincide with the curves of $p^2/2 = A^2(t)/2$] and is also well consistent with the analysis using the Wigner function by Czirják *et al.* for the ionization process of an atom in a static electric field [19]. In addition, it should be pointed out that, though a $\sin^2$ temporal envelope is used for the laser pulse here, which is different from the physical envelope (usually a Gaussian envelope) used in the experiment, our calculation with a Gaussian temporal envelope (not shown here) shows that the effects discussed in this paper are independent of the pulse envelope since these effects focus on the low-energy part of the ATI spectrum and are mainly determined by the crest part of the laser pulse, significantly different from the high-energy part of the ATI spectrum discussed in Refs. [12,20].

Furthermore, we show the time-energy distribution (in Fig. 4) of electrons emitted by laser pulses with the same parameters as those in Fig. 2(e), except the initial phase $\varphi = \pi/2$. It is clearly shown that the interference structures in Fig. 4 appear at two positions $t = 1.75$ and 2.25 o.c. Moreover, different from the case of $\varphi = 0$, since those electrons, which are ionized around $t = 1.5$, 2.0, and 2.5 o.c., contribute significantly to the spectrum, the interferences become more complicated, and the energy spectrum (solid line in Fig. 4) shows more complicated structures. However, one can find that the interference structures at $t = 1.75$ and 2.25 o.c. are similar to those in Figs. 2(e) and 2(f), respectively, since the structures of the strips started at $t = 1.5$ and 2.0 o.c.

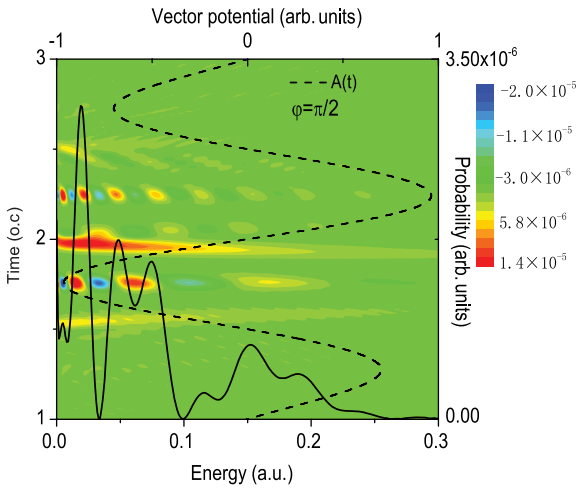

FIG. 4. (Color online) Time-energy distribution and energy spectrum of an electron emitted in few-cycle laser pulses with the same parameters as those in Fig. 2(e), except the initial phase $\varphi = \pi/2$. The solid line is the energy spectrum, and the dashed line is the vector potential.

and the strips started at $t = 2.0$ and 2.5 o.c. resemble those started at $t = 1.75$ and 2.25 o.c. in Fig. 2(e) and those started at $t = 1.75$ and 2.25 o.c. in Fig. 2(f), respectively. In addition, the spectrum is symmetrical with respect to the direction of electron momentum in accordance with the ionization probability distribution, electric amplitude, and vector potential shown in Fig. 1(f) [the electric amplitude satisfies $\mathbf{E}(t) = \mathbf{E}(4T - t)$, and the vector potential satisfies $\mathbf{A}(t) = -\mathbf{A}(4T - t)$].

IV. CONCLUSION

In conclusion, we use a Wigner-distribution-like function to study the time-energy distribution of a photoelectron emitted from an atom in few-cycle laser fields with different frequencies. The WDL function enables us to show the time distribution of the ionization probability. With a decreasing laser frequency, the time distribution of ionization probability becomes more and more peaking at the crests of electric amplitude of the laser pulse, which explicitly demonstrates the transition of the ionization process from the multiphoton regime to the tunneling regime. Accompanying this transition, the semiclassical picture of the ATI process, which relies on a correspondence between the final drift momentum and the ionization time, becomes asymptotically valid and agrees well with the time-energy distribution in the tunneling regime. Especially, the semiclassical picture is already available when $\gamma \sim 1$ even though the disagreement between the quantum time-energy distribution and the semiclassical calculation is noticeable. Meanwhile, the photoelectron energy spectrum changes from a smooth distribution to a spectrum with abundant fine structures and is more and more dependent on the direction of the ejection of the photoelectron and carrier-envelope phase of the laser field. The WDL function enables us to explicitly attribute the fine structure in the tunneling regime to interference between electrons with the same kinetic energy ejected at different times.

ACKNOWLEDGMENTS

This work was partially supported by the National Basic Research Program of China (Grant No. 2011CB8081002), NNSFC (Grants No. 11074026, No. 11175227, and No. 11105205), and the Shanghai Supercomputer Center of China.

[1] L. V. Keldysh, Zh. Eksp. Teor. Fiz. **47**, 1945 (1964).
[2] P. Agostini, F. Fabre, G. Mainfray, G. Petite, and N. K. Rahman, Phys. Rev. Lett. **42**, 1127 (1979).
[3] H. B. van Linden van den Heuvell, and H. G. Muller, *Multiphoton Processes*, edited by S. J. Smith and P. L. Knight (Cambridge University Press, Cambridge, UK, 1988), p. 25.
[4] U. Mohideen, M. H. Sher, H. W. K. Tom, G. D. Aumiller, O. R. Wood, II, R. R. Freeman, J. Bokor, and P. H. Bucksbaum, Phys. Rev. Lett. **71**, 509 (1993).
[5] G. G. Paulus, W. Nicklich, H. Xu, P. Lambropoulos, and H. Walther, Phys. Rev. Lett. **72**, 2851 (1994).
[6] P. B. Corkum, Phys. Rev. Lett. **71**, 1994 (1993).
[7] C. I. Blaga, F. Catoire, P. Colosimo, G. G. Paulus, H. G. Muller, P. Agostini, and L. F. Dimauro, Nat. Phys. **5**, 335 (2009).
[8] W. Quan, Z. Lin, M. Wu, H. Kang, H. Liu, X. Liu, J. Chen, J. Liu, X. T. He, S. G. Chen, H. Xiong, L. Guo, H. Xu, Y. Fu, Y. Cheng, and Z. Z. Xu, Phys. Rev. Lett. **103**, 093001 (2009).
[9] W. Becker *et al.*, Adv. At., Mol., Opt. Phys. **48**, 35 (2002).
[10] R. Kopold, W. Becker, M. Kleber, and G. G. Paulus, J. Phys. B **35**, 217 (2002).
[11] F. Lindner, M. G. Schätzel, H. Walther, A. Baltuška, E. Goulielmakis, F. Krausz, D. B. Milošević, D. Bauer, W. Becker, and G. G. Paulus, Phys. Rev. Lett. **95**, 040401 (2005).
[12] F. Lindner, G. G. Paulus, H. Walther, A. Baltuška, E. Goulielmakis, M. Lezius, and F. Krausz, Phys. Rev. Lett. **92**, 113001 (2004).
[13] F. M. H. Faisal, J. Phys. B **6**, L89 (1973).
[14] H. R. Reiss, Phys. Rev. A **22**, 1786 (1980).
[15] V. P. Krainov, J. Opt. Soc. Am. B **14**, 425 (1997).
[16] L. Guo, S. S. Han, and J. Chen, Opt. Express **18**, 1240 (2010).
[17] See, e.g., S. F. J. Larochelle, A. Talebpoury, and S. L. Chin, J. Phys. B **31**, 1215 (1998); J. Chen, J. Liu, and S. G. Chen, Phys. Rev. A **61**, 033402 (2000).
[18] V. C. Reed and K. Burnett, Phys. Rev. A **43**, 6217 (1991).
[19] A. Czirják, R. Kopold, W. Becker, M. Kleber, and W. P. Schleich, Opt. Commun. **179**, 29 (2000).
[20] C. Altucci, V. Tosa, R. Velotta, and C. H. Nam, Phys. Rev. A **70**, 065402 (2004).